Nonrandom behavior in multicomponent lattice mixtures: Effects of solute size and shape

G. L. Aranovich, T. Hocker, D. W. Wu, and M. D. Donohue

Citation: The Journal of Chemical Physics **106**, 10282 (1997); doi: 10.1063/1.474065
View online: http://dx.doi.org/10.1063/1.474065
View Table of Contents: http://scitation.aip.org/content/aip/journal/jcp/106/24?ver=pdfcov
Published by the AIP Publishing

Nonrandom behavior in multicomponent lattice mixtures: Effects of solute size and shape

G. L. Aranovich, T. Hocker, D. W. Wu, and M. D. Donohue[a)]
Department of Chemical Engineering, The Johns Hopkins University, Baltimore, Maryland 21218

(Received 5 December 1996; accepted 19 March 1997)

A new lattice theory is proposed to describe nonrandom behavior for multicomponent mixtures of monomers, for mixtures of monomers interacting with a polymer, and for mixtures of monomers at a surface. Based on concepts first proposed by Ono and Kondo, this new approach allows one to derive local densities around each species taking into account molecular interactions as well as molecular geometry and lattice structure. This approach can be used to describe a number of very different systems in the framework of a single model. The generalizations presented here are rigorous in that no assumptions beyond those of the original (binary) theory are needed in order to treat multicomponent mixtures of molecules of different sizes and shapes. © *1997 American Institute of Physics.* [S0021-9606(97)50724-0]

INTRODUCTION

In a previous paper,[1] a new approach was presented to predict the thermodynamic properties of a lattice gas by generalizing the ideas of Ono and Kondo[2,3] to treat a lattice in three dimensions. Here we extend this theory to treat multicomponent mixtures of monomers, mixtures containing monomers and a polymer, and monomers at a surface. Expressions for local densities around each species are derived which take into account molecular interactions as well as molecular geometry and lattice structure. It is shown that expressions can be written in the same general form for mixtures of monomers, monomers interacting with a polymer, and monomers at a surface. Since this theory relies on an assumption of mean-field behavior,[3] it is not an exact solution for the Ising model in three dimensions. However, the generalizations presented here are rigorous in that no assumptions are needed beyond those used to derive expressions for binary mixtures in order to treat multicomponent mixtures of molecules of different sizes and shapes.

NONRANDOM BEHAVIOR IN MULTICOMPONENT LATTICE MIXTURES

In the lattice theory considered here, vibrations of molecules around their equilibrium positions and other kinetic effects are neglected. The quasicrystalline lattice contains ν different kinds of monomers. There are interactions between nearest neighbors with the energy of interaction for an i-j pair being designated by ϵ_{ij}. Here, the values for ϵ_{ij} are negative for attractive forces. An arbitrary molecule of type j will be considered as a central (i.e., reference) molecule. Consider exchanging a molecule of type i in the first shell of j with a molecule of type l at a site infinitely distant from j, i.e.,

$$M_i^j + M_l^\infty \rightarrow M_i^\infty + M_l^j . \tag{1}$$

Note that in the above expression, and in all other equations, the subscript letter denotes the type and the superscript letter the site of a certain molecule. Hence M_i^j is a molecule of species i adjacent to a reference molecule of species j. If this exchange occurs at local equilibrium under constant temperature and volume,

$$\Delta U - T\Delta S = 0, \tag{2}$$

where ΔU and ΔS are the energy and entropy changes, and T is the absolute temperature. In the microcanonical ensemble, the value of ΔS is represented in the form

$$\Delta S = k_B \ln\left(\frac{W_1}{W_2}\right), \tag{3}$$

where W_1 is the number of configurations for the system with the molecule i in the first shell of j and the molecule l is at a site infinitely distant from the reference molecule. W_2 is then the number of configurations for the system with the molecule l in the first shell of j and the molecule i is at a site infinitely distant from the reference molecule. k_B denotes the Boltzmann constant.

If the total number of configurations for the system is W_t, and assuming a finite correlation length, the probability for *state 1*, and the probability for *state 2* are approximated by

$$P_1 = \frac{W_1}{W_t} = x_i^j x_l^\infty , \tag{4}$$

and

$$P_2 = \frac{W_2}{W_t} = x_l^j x_i^\infty , \tag{5}$$

where x_i^j is the probability for having a molecule of type i in the first shell of the reference molecule of type j, and x_i^∞ is the probability for having a molecule of type i in the bulk. For any j we have the constraint

$$x_1^j + x_2^j + \ldots + x_\nu^j = 1. \tag{6}$$

[a)]Author to whom correspondence should be addressed.

The probabilities, x, should not be confused with mole fractions in off-lattice systems since here x takes into account the number of holes. Rather, x is equivalent to the density in off-lattice systems. Substituting Eqs. (4) and (5) into Eq. (3) gives

$$\Delta S = S_1 - S_2 = k_B \ln\left(\frac{x_i^j}{x_i^\infty}\frac{x_l^\infty}{x_l^j}\right). \tag{7}$$

Calculating the change in energy requires specification of the lattice type and coordination number, z. Here we assume a cubic lattice ($z=6$) and, for simplicity, we assume that the compositions of the solution in the second and more distant shells do not differ from those in the bulk. Both of these assumptions can be relaxed,[1,4] but the mathematical complexity increases. The change in energy can be calculated by assuming the mean-field approximation[3] for molecules adjacent to the reference molecule, and the Bragg–Williams[5] approximation for molecules infinitely distant from the reference molecule. The energy is the sum over all possible nearest-neighbor interactions, i.e.,

$$\Delta U = -(U_1 - U_2) = -\left[\epsilon_{ij} - \epsilon_{lj} + \sum_{m=1}^{\nu} x_m^\infty(\epsilon_{lm} - \epsilon_{im})\right]. \tag{8}$$

Note that we have changed the sign in Eq. (8) since attractive interactions between molecules are defined as having negative interaction energies. From Eq. (2) and Eqs. (7) and (8) it follows that

$$k_B T \ln\left(\frac{x_i^j}{x_i^\infty}\frac{x_l^\infty}{x_l^j}\right) + \epsilon_{ij} - \epsilon_{lj} - \sum_{m=1}^{\nu} x_m^\infty(\epsilon_{im} - \epsilon_{lm}) = 0. \tag{9}$$

Equation (9) represents a set of Ono–Kondo equations for a multicomponent mixture of monomers, where the indices i, j, and l denote the ν different monomers in the mixture. This extends the model for a binary system presented earlier[1] to an arbitrary number of components without any additional assumptions. Equation (9) can be used to calculate local probabilities (or densities) for a lattice mixture. From Eq. (6), x_i^j can be written as

$$x_i^j = \frac{1}{\sum_{l=1}^{\nu} x_l^j / x_i^j}, \tag{10}$$

and Eq. (9) can be rearranged so that

$$\frac{x_l^j}{x_i^j} = \frac{x_l^\infty}{x_i^\infty}\exp\left\{\left[\epsilon_{ij} - \epsilon_{lj} + \sum_{m=1}^{\nu} x_m^\infty(\epsilon_{lm} - \epsilon_{im})\right] \Big/ k_B T\right\}. \tag{11}$$

Hence in the framework of the Ono–Kondo lattice model, the probability for having a molecule i next to some reference site j is given by

$$x_i^j = \frac{x_i^\infty}{\sum_{l=1}^{\nu} x_l^\infty \exp\{[\epsilon_{ij} - \epsilon_{lj} + \sum_{m=1}^{\nu} x_m^\infty(\epsilon_{lm} - \epsilon_{im})]/k_B T\}}. \tag{12}$$

INTERNAL ENERGY

Equation (12) can be used to calculate the configurational energy for a multicomponent, nonrandom lattice mixture. In a quasicrystalline lattice, where the molecules are assumed to sit in a regular array in space and where second neighbor and longer-range interactions are neglected, U can be written in the form

$$U = \frac{z}{2} N\left(\sum_{i=1}^{\nu} x_i^\infty \epsilon_{ii} + \frac{1}{4}\sum_{i=1}^{\nu}\sum_{j=1}^{\nu} P_{ij}\Delta_{ij}\right), \tag{13}$$

where P_{ij} denotes the fraction of i-j bonds, N is the total number of lattice sites, z is the coordination number, and Δ_{ij} is the interchange energy,

$$\Delta_{ij} = 2\epsilon_{ij} - \epsilon_{ii} - \epsilon_{jj}. \tag{14}$$

The single sum in Eq. (13) represents the sum of the internal energies of the pure components and the double sum is the energy change due to mixing. By applying the concept of conditional probabilities, the fraction of i-j bonds, P_{ij}, can be written as

$$P_{ij} = P_{ji} = x_j^\infty x_i^j + x_i^\infty x_j^i. \tag{15}$$

Inserting Eq. (15) into Eq. (13) leads to

$$U = \frac{z}{2} N\left(\sum_{i=1}^{\nu} x_i^\infty \epsilon_{ii} + \frac{1}{2}\sum_{i=1}^{\nu}\sum_{j=1}^{\nu} x_j^\infty x_i^j \Delta_{ij}\right). \tag{16}$$

It is shown in Appendix A that $x_j^\infty x_i^j$ must equal $x_i^\infty x_j^i$ at all conditions. However, this constraint may not be satisfied, when x_i^j and x_j^i are calculated by an approximate theory. Therefore, since the Ono–Kondo model is only an approximation for the Ising lattice model,[5] $x_j^\infty x_i^j \approx x_i^\infty x_j^i$, and Eq. (16) averages $x_j^\infty x_i^j$ and $x_i^\infty x_j^i$. See Appendix A for a more detailed discussion on this subject. Combining Eqs. (12) and (16), we obtain

$$U = U_{\text{pure}} + \frac{z}{4} N\sum_{i=1}^{\nu}\sum_{j=1}^{\nu} x_i^\infty x_j^\infty \Delta_{ij}\Psi_{ij}, \tag{17}$$

where U_{pure} is the sum of the internal energies of the pure components,

$$U_{\text{pure}} = \frac{z}{2} N\sum_{i=1}^{\nu} x_i^\infty \epsilon_{ii} \tag{18}$$

and Ψ_{ij} is defined as

$$\Psi_{ij} \equiv \frac{x_i^j}{x_i^\infty} = \frac{\exp[(-\epsilon_{ij} + \sum_{m=1}^{\nu} x_m^\infty \epsilon_{im})/k_B T]}{\sum_{l=1}^{\nu} x_l^\infty \exp[(-\epsilon_{lj} + \sum_{m=1}^{\nu} x_m^\infty \epsilon_{lm})/k_B T]}. \tag{19}$$

Note that in the case of a completely random mixture (i.e., in the Bragg–Williams approximation), Ψ_{ij} is unity. Hence, Ψ_{ij} is measure of the deviations of a nonrandom system from its ''ideal'' random limit. Furthermore, the constraint $x_j^\infty x_i^j = x_i^\infty x_j^i$ requires Ψ to be symmetric, i.e., $\Psi_{ij} = \Psi_{ji}$, which is satisfied only approximately by Eq. (19). Table I shows results for Ψ for a pure lattice gas (i.e., a mixture of

TABLE I. Values for Ψ for a pure lattice gas for different bulk densities and interaction energies.

ϵ_{AA}/k_BT	-0.1		-0.5		-1	
x_A^∞	Ψ_{AH}	Ψ_{HA}	Ψ_{AH}	Ψ_{HA}	Ψ_{AH}	Ψ_{HA}
0.00	1.000	1.000	1.000	1.000	1.000	1.000
0.10	0.991	0.991	0.956	0.946	0.914	0.873
0.20	0.984	0.984	0.922	0.910	0.850	0.803
0.30	0.979	0.979	0.898	0.888	0.803	0.767
0.40	0.976	0.976	0.883	0.877	0.772	0.753
0.50	0.975	0.975	0.876	0.876	0.755	0.755
0.60	0.976	0.976	0.877	0.883	0.753	0.772
0.70	0.979	0.979	0.888	0.898	0.767	0.803
0.80	0.984	0.984	0.910	0.922	0.803	0.850
0.90	0.991	0.991	0.946	0.956	0.873	0.914
1.00	1.000	1.000	1.000	1.000	1.000	1.000

A-monomers and *H*-holes) for three different *AA* interaction energies as a function of bulk density calculated from Eq. (19).

It has already been shown that the Ono–Kondo lattice model gives excellent predictions for binary mixtures and for a lattice gas with holes.[1] Here we demonstrate its accuracy for multicomponent mixtures. Figure 1 shows analytical solutions and computer simulations for a ternary mixture in a cubic lattice ($z=6$) in three different ways. The mixture consists of *A*-monomers, *B*-monomers, and *H*-holes. The bulk density of *B*-monomers is held constant at $x_B^\infty=0.2$, so that varying the bulk concentration of *A*-monomers implies a variation in the number of holes. In order to obtain dimensionless expressions for internal energies, we define an average kinetic energy, $U_{\rm kin}=k_BT(N_A+N_B)z/2$.

In Fig. 1(a), the dimensionless internal energies for the nonrandom system, $\widetilde{U}=U/U_{\rm kin}$, and for the random system, $\widetilde{U}_{RM}=U_{RM}/U_{\rm kin}$, are shown as a function of the bulk density of *A*-monomers, x_A^∞. In Fig. 1(b), the ratio of the internal energy for the nonrandom system to the internal energy for the random system, $\widetilde{U}/\widetilde{U}_{RM}$, is plotted as a function of x_A^∞. Figure 1(c) shows the difference between the internal energy of the nonrandom and the random system, $\widetilde{U}-\widetilde{U}_{RM}$, as a function of x_A^∞. Equation (17) is used at the conditions given in Table II for the analytical calculations (represented as lines). The symbols represent Monte Carlo simulations for molecules on a lattice at the same conditions.

The key point here is the good agreement between theory and simulation. The largest difference for $\widetilde{U}$ between the model, Eq. (17), and Monte Carlo simulations is 1.7%. Figure 1(c) shows that this error is largest when the difference between $\widetilde{U}$ and $\widetilde{U}_{RM}$ is largest. For attractive interactions between molecules, the internal energy of mixing, $\Delta\widetilde{U}_{\rm mix}$, is a positive function, since energy has to be supplied from the surroundings in order to ''dilute'' the energetically favorable *A*-*B* mixture with ''neutral'' holes. The amount of energy supplied has to be higher for a random system than for a nonrandom system, since the latter is able to form energetically favorable clusters of *A*- and *B*-monomers. As a consequence, the absolute value of the internal energy for the nonrandom mixture is higher than the one for the random mixture.

In addition, several things are evident from the graphs in Fig. 1. For high densities, $\widetilde{U}$ approaches $\widetilde{U}_{RM}$ asymptotically. Since Δ_{AB} is equal to zero, the value of $\widetilde{U}$ at the high density limit is given by $\widetilde{U}=x_B^\infty\epsilon_{BB}/k_BT+(1-x_B^\infty)\epsilon_{AA}/k_BT$. Furthermore, $\widetilde{U}$ and $\widetilde{U}_{RM}$ do not approach zero as x_A^∞ approaches zero. This is due to the number of *B*-monomers being held constant. Also, Fig. 1(b) shows that $\widetilde{U}/\widetilde{U}_{RM}$ goes through a maximum and approaches unity at high x_A^∞. This behavior results from the fact that *A*-*A* and *A*-*B* interactions are stronger than *B*-*B* interactions. Therefore, the mixture becomes more structured by adding *A*-monomers. However, for high bulk densities the mixture has to approach random behavior. It also should be noted that the intercept at $x_A^\infty=0$ is much less than the Boltzmann factor of $\exp(-\epsilon_{AA}/k_BT)=2.01$ as would be the case for a pure lattice gas mixture of *A* molecules with holes. Again, this is because the calculations are for a ternary system.

MONOMER–POLYMER INTERACTIONS

Here we consider a straight polymer chain at a fixed position in a $\nu-1$ component solution of monomers. *A priori*, this polymer occupies the sites with $k_x=k_y=0$, where k_x, k_y, and k_z are the lattice coordinates in three dimensions. Therefore, the first shell of molecules around this polymer are lattice sites with $k_x=\pm1$ and $k_y=\pm1$. For a cubic lattice, each monomer molecule in the first shell adjacent to the polymer has two neighbors in the same shell. With these assumptions, Eq. (9) can be rewritten for the case of an infinitely dilute polymer in a monomer solution as

$$k_BT\ln\left(\frac{x_i^p}{x_i^\infty}\frac{x_l^\infty}{x_l^p}\right)+\epsilon_{ip}-\epsilon_{lp}+2\sum_{m=1}^{\nu-1}x_m^p(\epsilon_{im}-\epsilon_{lm})-3\sum_{m=1}^{\nu-1}x_m^\infty(\epsilon_{im}-\epsilon_{lm})=0, \tag{20}$$

where the superscript *p* denotes the first shell of the polymer (which is the νth component). Unlike Eq. (9), Eq. (20) is

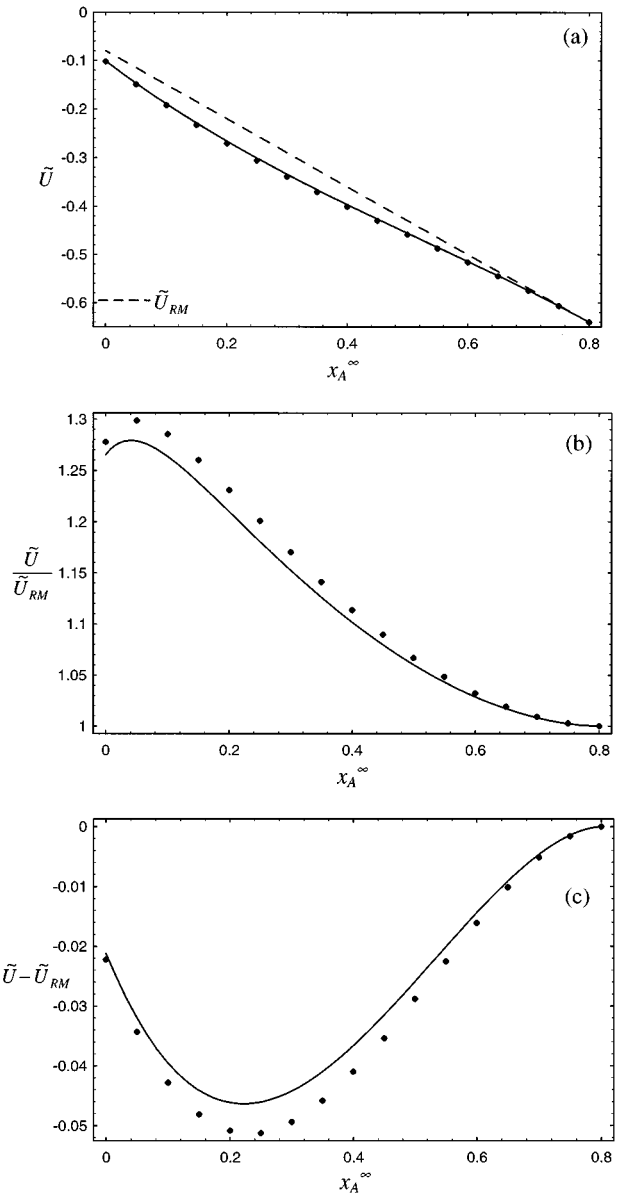

FIG. 1. Presented are analytical calculations and computer simulations of internal energies for a ternary lattice mixture (i.e., *A*-monomers, *B*-monomers, and *H*-holes), where the number of *B*-monomers is held constant at $x_B^\infty=0.2$. (a) The dimensionless internal energy for the nonrandom system, $\tilde{U}=U/U_{\rm kin}$, and the dimensionless internal energy for the random system, $\tilde{U}_{RM}=U_{RM}/U_{\rm kin}$, as a function of the bulk density of *A*-monomers, x_A^∞. (b) The ratio of the internal energy for the nonrandom to the random system, $\tilde{U}/\tilde{U}_{RM}$, is plotted as a function of x_A^∞. (c) The difference between the internal energy of the nonrandom and the random system, $\tilde{U}-\tilde{U}_{RM}$, is given as a function of x_A^∞. For the analytical calculations (represented as lines), Eq. (17) is used at the conditions given in Table II. The points represent Monte Carlo simulations for molecules on a lattice.

transcendental in x_i^p and x_l^p. For a $(\nu-1)$-component mixture of monomers, there are $(\nu-2)$ independent equations of this form, but Eq. (6) gives an additional constraint. Unless further assumptions are made, these equations must be solved by numerical techniques.

TABLE II. Parameters for Figs. 1(a), 1(b), and 1(c).

Species	Bulk concentrations	Interaction energies
A-monomers	x_A^∞	$\epsilon_{AA}=-0.7k_BT,\ \epsilon_{AB}=-0.55k_BT,\ \epsilon_{AH}=0$
B-monomers	$x_B^\infty=0.2$	$\epsilon_{BB}=-0.4k_BT,\ \epsilon_{BH}=0$
H-holes	$x_H^\infty=0.8-x_A^\infty$	$\epsilon_{HH}=0$

INTERNAL ENERGY FOR A POLYMER IN A MIXTURE OF MONOMERS

As shown above for a monomer system, the Ono–Kondo equation (20) can be used in the same manner to determine the configurational energy for a nonrandom mixture containing a polymer chain. Since the configurational energy is the sum of all nearest-neighbor interactions, for this system, U can be written as

$$U=\left(\frac{1}{2}+\frac{1}{2}\,\delta_{ij}\right)\sum_{i=1}^{\nu-1}\sum_{j=1}^{\nu-1}N_{ij}\epsilon_{ij}+\sum_{i=1}^{\nu-1}N_{ip}\epsilon_{ip}. \tag{21}$$

Here, N_{ij} is the total number of $i-j$ bonds and N_{ip} the total number of bonds between a segment of the polymer chain and a monomer of species i. δ_{ij} denotes the Kronecker delta, defined as

$$\delta_{ij}\equiv\begin{cases}1, & i=j\\ 0, & i\neq j\end{cases}. \tag{22}$$

In Eq. (21), we consider only a single straight polymer molecule of infinite length, i.e., no interactions between polymer segments and no end effects for the polymer are taken into account. The conservation principle for monomers of an arbitrary species i is given by

$$\frac{z}{2}\,N_i=\left(\frac{1}{2}+\frac{1}{2}\,\delta_{ij}\right)\sum_{j=1}^{\nu-1}N_{ij}+\frac{1}{2}\,N_{ip}. \tag{23}$$

With Eq. (23), Eq. (21) can be written as

$$U=\frac{z}{2}\,N\left[\sum_{i=1}^{\nu-1}x_i^\infty\epsilon_{ii}+\frac{1}{2}\sum_{i=1}^{\nu-1}\sum_{j=1}^{\nu-1}x_j^\infty x_i^j\Delta_{ij}+\sum_{i=1}^{\nu-1}x_i^p\left(\epsilon_{ip}-\frac{1}{2}\,\epsilon_{ii}\right)\right]. \tag{24}$$

Note that Eq. (24) is similar to Eq. (16) except for the last sum in Eq. (24), which takes into account interactions between monomers and polymer segments. To obtain an explicit expression for U,x_i^j can be calculated analytically from Eq. (12) and x_i^p can be calculated numerically from Eq. (20).

MONOMERS AT A SURFACE

For molecules adsorbed at a surface, each molecule interacting with the surface has four other neighbors in the same layer, and has one neighbor in the second layer. In the framework of the Ono–Kondo lattice model, this geometry leads to

$$k_B T \ln\left(\frac{x_i^s}{x_i^\infty}\frac{x_l^\infty}{x_l^s}\right)+\epsilon_{is}-\epsilon_{ls}+4\sum_{m=1}^{\nu} x_m^s(\epsilon_{im}-\epsilon_{lm})$$

$$-5\sum_{m=1}^{\nu} x_m^\infty(\epsilon_{im}-\epsilon_{lm})=0. \tag{25}$$

Equation (25) represents the Ono–Kondo equation for a multicomponent monomer system at a surface where the indices i and l denote the ν different monomers. It therefore extends the Ono–Kondo equation for a binary system at a surface, which was presented earlier,[6] to an arbitrary number of components.

GENERAL FORM OF EQUATIONS FOR LOCAL DENSITIES IN MULTICOMPONENT LATTICE MIXTURES

It can be seen that Eqs. (9), (20), and (25) have the same structure and can therefore be written in a more general form

$$k_B T \ln\left(\frac{x_i^\lambda}{x_i^\infty}\frac{x_l^\infty}{x_l^\lambda}\right)+\epsilon_{i\lambda}-\epsilon_{l\lambda}+K_1\sum_{m=1}^{\nu} x_m^\lambda(\epsilon_{im}-\epsilon_{lm})$$

$$-(z-K_2)\sum_{m=1}^{\nu} x_m^\infty(\epsilon_{im}-\epsilon_{lm})=0, \tag{26}$$

where K_1 is the number of first-shell neighbors for a molecule in the first shell, and K_2 is the number of bonds to the bulk for a molecule in the first shell. The type of reference site is denoted by the superscript λ.

It should be noted that Eq. (26) reduces to an expression similar to the Langmuir adsorption isotherm for $\lambda=S$ (surface), $K_1=0$ and $K_2=z$, which implies a neglect of self-interactions among the monomers. Likewise, Eq. (26) reduces to the Frumkin adsorption isotherm for $\lambda=S$ (surface), $K_1=4$, and $K_2=z$, implying that $x_A^\lambda \gg x_A^\infty$.

Figure 2 shows a comparison of the Ono–Kondo, Frumkin, and Langmuir adsorption isotherms together with Monte Carlo simulations for molecules on a lattice.

Table III gives parameters for Eq. (26) for a cubic lattice for four different cases that are treated in the discussion below. It shows the dependence of K_1 and K_2 on the geometry of the reference site (monomer, polymer, surface) and the corresponding values for λ.

DISCUSSION

The model presented above can be used to calculate local densities and configurational energies for a variety of systems. However, despite the similarity of the equations for ''adsorption'' of monomers around monomers, monomers around a polymer, and monomers at a surface, the behavior of these systems is not isomorphic. This is illustrated in Fig. 3. Plotted are the ratios of densities in the first shell of some reference site λ to the density of A-monomers in the bulk, x_A^λ/x_A^∞, as a function of x_A^∞. Calculations are shown for four systems by applying Eq. (26) and the values given in Table III [the application of Eq. (26) to the systems shown in Table III is given in Appendix B]. Also shown in Fig. 3 are results

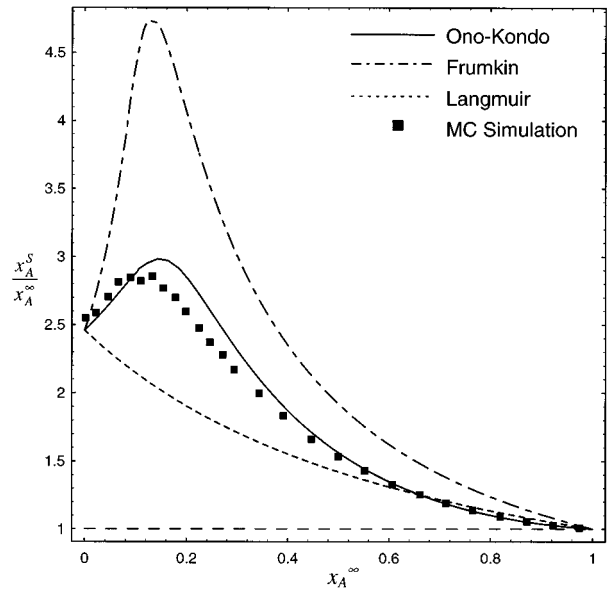

FIG. 2. Presented are analytical solutions and computer simulations for a lattice gas (i.e., a mixture of A-monomers and H-holes) where A-monomers are adsorbed in the first layer at a surface. Ratios of local densities at the surface to bulk densities, x_A^S/x_A^∞, are shown as a function of the bulk density, x_A^∞. For the analytical calculations (represented as lines) Eq. (26) is used with different sets of parameters. The Ono–Kondo monolayer adsorption isotherm is obtained for $\lambda=S$ (surface), $K_1=4$, and $K_2=1$. The Langmuir adsorption isotherm is obtained for $\lambda=S$, $K_1=0$, and $K_2=z$, and the Frumkin adsorption isotherm for $\lambda=S$, $K_1=4$, and $K_2=z$. The points represent Monte Carlo simulations for molecules on a lattice. The surface-molecule interaction energy is $\epsilon_{AS}=-0.9\,k_BT$, and the molecule–molecule interaction energy is $\epsilon_{AA}=-0.6\,k_BT$.

for Monte Carlo simulations on a lattice for monomers around monomers and monomers at a surface.

Case AA is for a mixture of A-monomers and H-holes, i.e., a lattice gas. The calculations show the ratio of local densities of A molecules around a central A molecule ($\lambda=A$) to the bulk density x_A^∞, as a function of x_A^∞. The other three cases also consist of a mixture of A-monomers and H-holes in the bulk. However, in addition, we consider different ''solutes'' (B-monomers, P-polymer, S-surface). Case AB shows local densities of A-monomers around a B-monomer ($\lambda=B$) at infinite dilution. Case AP shows local densities of A-monomers around a polymer ($\lambda=P$) and case AS shows local densities of A-monomers at a surface ($\lambda=S$). In each case the ''solute''-solvent interaction energies are equal to the solvent–solvent interaction energies, i.e., $\epsilon_{AA}=\epsilon_{AB}=\epsilon_{AP}=\epsilon_{AS}=-0.6k_BT$, and they are slightly above the classical critical temperature for a cubic lattice

TABLE III. Parameters for Eq. (26).

System	Case	λ	K_1	K_2
A-monomer around A-monomer (solvent)	AA	A	0	5
A-monomer around B-monomer (solute)	AB	B	0	5
A-monomer around polymer-segment	AP	P	2	3
A-monomer at surface	AS	S	4	1

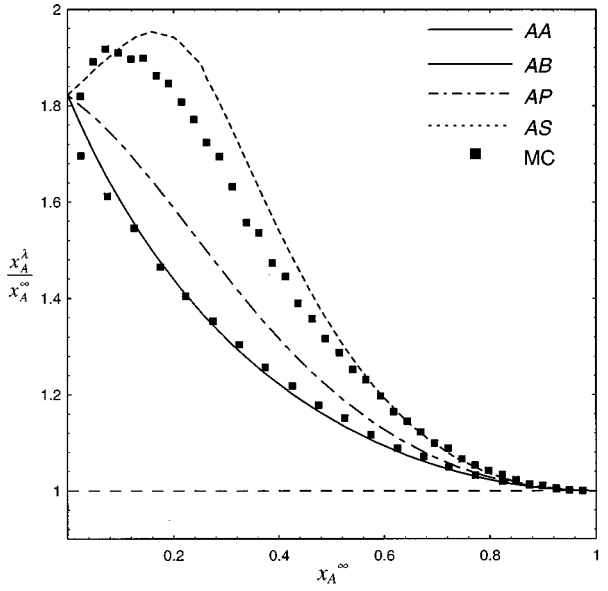

FIG. 3. Presented are analytical solutions and computer simulations for a lattice gas (i.e., A-monomers and holes in the bulk) where A-monomers are absorbed in the first layer adjacent to different ''solutes.'' Ratios of local densities to bulk densities, x_A^λ/x_A^∞, are shown as a function of the bulk density, x_A^∞. Case AA represents the local densities of A-monomers around A-monomers ($\lambda=A$). The other three cases show local densities of A-monomers around different ''solutes'' (B-monomer, P-polymer, S-surface). Case AB marks the local densities of A-monomers around a B-monomer ($\lambda=B$) in infinite dilution. Case AP represents the local densities of A-monomers around a P-polymer ($\lambda=P$) in infinite dilution and case AS shows the local densities of A-monomers at a S-surface ($\lambda=S$). For the analytical calculations (represented as lines) Eq. (26) is used with the values given in Table III. The points represent Monte Carlo simulations for molecules on a lattice. In each case the ''solute''-solvent interaction energies are equal to the solvent–solvent interaction energies, i.e., $\epsilon_{AA}=\epsilon_{AB}=\epsilon_{AP}=\epsilon_{AS}=-0.6k_BT$. The curves for case AA and case AB are the same since both types of molecules are identical in energy and shape. The agreement between the model and Monte Carlo simulations for monomer–monomer self-interactions is quite good. The results for monolayer adsorption at a surface suggests that the theoretical predictions of the fourth virial coefficient may be in error.

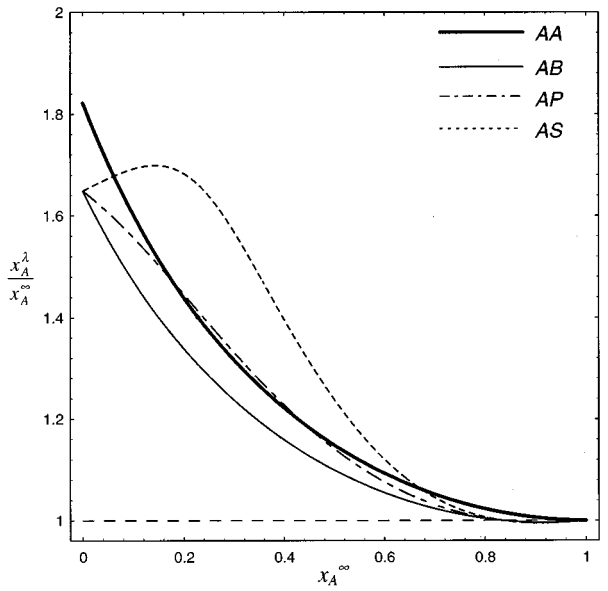

FIG. 4. Presented are analytical solutions for a lattice gas (i.e., A-monomers and holes in the bulk) where A-monomers are adsorbed in the first layer of different reference sites. Ratios of local densities to bulk densities, x_A^λ/x_A^∞, are shown as a function of the bulk density, x_A^∞. Case AA represents the local densities of A-monomers around A-monomers ($\lambda=A$). The other three cases show local densities of A-monomers around different ''solutes'' (B-monomer, P-polymer, S-surface). Case AB represents the local densities of A-monomers around a B-monomer ($\lambda=B$) in infinite dilution. Case AP represents the local densities of A-monomers around a P-polymer ($\lambda=P$) in infinite dilution and case AS shows the local densities of A-monomers at a S-surface ($\lambda=S$). For the analytical calculations Eq. (26) is used with the values in Table III. The A-monomer self-interactions are the same than in Fig. 3, but the interactions between A-monomers and ''solutes'' (B-monomers, P-polymer, S-surface) now are slightly weaker, i.e., $\epsilon_{AB}=\epsilon_{AP}=\epsilon_{AS}=-0.5k_BT$ and $\epsilon_{AA}=-0.6k_BT$.

($\epsilon/k_BT_C=-2/3$). As expected, the curves for case AA and case AB cannot be distinguished from each other since $\epsilon_{AA}=\epsilon_{AB}$ and both types of molecules have the same shape. Note that all four systems have Boltzmann weighted interactions and go to the Boltzmann factor, i.e., $\exp(-\epsilon_{A\lambda}/k_BT)=1.822$, at the low density limit. All curves approach asymptotically random behavior at high densities, and all systems satisfy the ''pure-component'' limit of having each site occupied by A-monomers. However, at intermediate bulk densities the local monomer density is higher near a solid surface than it is near a polymer, and this is higher than it is near a monomer. This enhanced ''adsorption'' occurs even without including the change in the potential of mean force,[5] and it becomes even larger if this effect is included.

Figure 4 shows similar calculations for a lattice gas of A-monomers and H-holes in the bulk where the A-monomer self-interactions now are slightly stronger than the interactions between A-monomers and ''solutes'' (B-monomers, P-polymer, S-surface), i.e., $\epsilon_{AB}=\epsilon_{AP}=\epsilon_{AS}=-0.5k_BT$ and $\epsilon_{AA}=-0.6k_BT$. As shown in Fig. 4, the ratio of AA local density to bulk density is the highest at low bulk densities. This is expected because this ratio of local density to bulk density goes to the Boltzmann factors when the bulk density approaches zero. At high bulk densities, the ratio of AA local density to the bulk density also is greater than the ratios of AB, AP, and AS local densities to the bulk density. Although not apparent in Fig. 4 this can be seen clearly in Fig. 5.

Figure 5 shows the difference between the local and bulk densities, $x_A^\lambda-x_A^\infty$, as a function of x_A^∞. Since it is assumed that the densities of A in the second and more distant shells of a reference site do not differ from those in the bulk, $x_A^\lambda-x_A^\infty$ is equal to the excess or Gibbs adsorption, $\Gamma_A(\lambda)$. In Fig. 5, all curves approach zero at both low density and high density. However, at intermediate bulk densities, the local densities near a polymer and near a surface can be greater than the AA local densities. This is due to geometric effects and it can occur even when the interaction energies are unfavorable. This is evident in both Figs. 4 and 5. At these intermediate densities, the shape of the ''solute'' is very important. Large solutes can have local densities that are significantly larger than random mixing due to the presence of

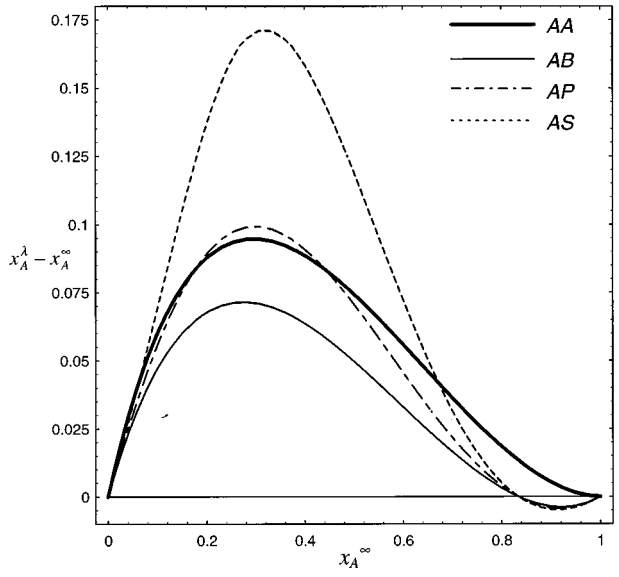

FIG. 5. Presented are analytical solutions for a lattice gas (i.e., A-monomers and holes in the bulk) where A-monomers are adsorbed in the first layer of different reference sites. Shown is the excess property $x_A^\lambda - x_A^\infty$ as a function of the bulk density, x_A^∞. Case AA represents the local densities of A-monomers around A-monomers ($\lambda = A$). The other three cases show local densities of A-monomers around different ''solutes'' (B-monomer, P-polymer, S-surface). Case AB represents the local densities of A-monomers around a B-monomer ($\lambda = B$) in infinite dilution. Case AP represents the local densities of A-monomers around a P-polymer ($\lambda = P$) in infinite dilution and case AS shows the local densities of A-monomers at a S-surface ($\lambda = S$). For the analytical calculations Eq. (26) is used with the values in Table III. The interaction energies are identical to those in Fig. 4, i.e., the A-monomer self-interactions are slightly stronger than the interactions between A-monomers and ''solutes'' (B-monomers, P-polymer, S-surface). The values are $\epsilon_{AB} = \epsilon_{AP} = \epsilon_{AS} = -0.5\ k_B T$ and $\epsilon_{AA} = -0.6\ k_B T$.

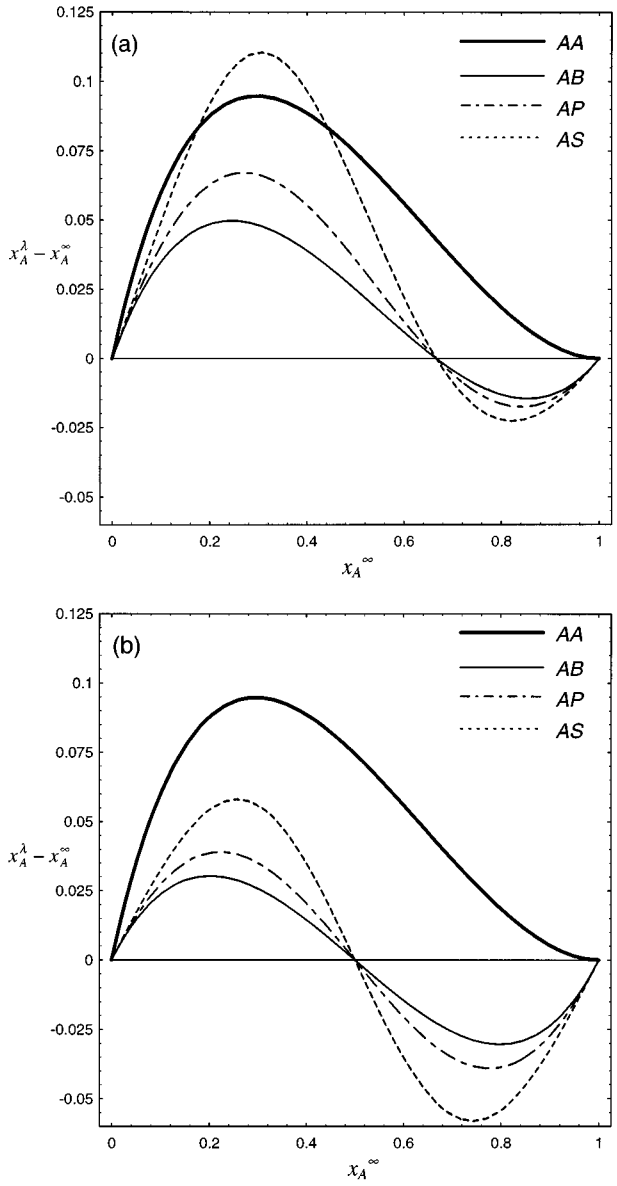

FIG. 6. Presented are analytical solutions for a lattice gas (i.e., A-monomers and holes in the bulk) where A-monomers are adsorbed in the first layer of different reference sites. Shown is the excess property $x_A^\lambda - x_A^\infty$, as a function of the bulk density, x_A^∞. Case AA represents the local densities of A-monomers around A-monomers ($\lambda = A$). The other three cases show local densities of A-monomers around different ''solutes'' (B-monomer, P-polymer, S-surface). Case AB represents the local densities of A-monomers around a B-monomer ($\lambda = B$) in infinite dilution. Case AP represents the local densities of A-monomers around a P-polymer ($\lambda = P$) in infinite dilution and case AS shows the local densities of A-monomers at a S-surface ($\lambda = S$). For the analytical calculations Eq. (26) is used with the values in Table III. In (a) and (b) the AA self-interactions are identical to those in Figs. 3, 4, and 5, i.e., $\epsilon_{AA} = -0.6 k_B T$, but the interactions between A-monomers and ''solutes'' (B-monomers, P-polymer, S-surface) are now weaker. In (a) the values are $\epsilon_{AB} = \epsilon_{AP} = \epsilon_{AS} = -0.4\ k_B T$ and in (b) the solvent-''solute'' interactions are $\epsilon_{AB} = \epsilon_{AP} = \epsilon_{AS} = -0.3\ k_B T$.

adsorbed molecules on neighbor sites. We believe this has implications in a variety of systems ranging from protein folding, to liquid crystals, to microphase separations in block co-polymers. This also has implications concerning the accuracy of models like the perturbed-hard-chain theory[7] which treat monomer/n-mer interactions as isomorphic to monomer–monomer interactions. Clearly, this assumption is not correct. However, it remains to be seen how large the errors are for real (off-lattice) systems.

Interestingly, for ''adsorption'' of A-monomers on ''solutes'' at high bulk densities, Fig. 5 shows negative values for the excess property $x_A^\lambda - x_A^\infty$. This is because the ''solute''-solvent interaction energies are slightly smaller than solvent–solvent interaction energies. Hence, at high bulk densities where the lattice is mostly filled with A-monomers, the holes adsorb on ''solute'' molecules preferentially despite the fact that ''solute''-solvent interactions are more favorable than hole-''solute'' interactions. This behavior is illustrated in Figs. 6 and 7.

Figure 6 shows the excess property $x_A^\lambda - x_A^\infty$ as a function of x_A^∞ for two cases where the solvent-''solute'' interactions are even weaker than in Fig. 5. It is obvious from both Figs. 6(a) and 6(b) that there is a significant enhancement of solvent molecules around ''solutes'' at low solvent densities and that there can be significant depletion of solvent around ''solutes'' at high solvent densities. Consequently, the enhancement and depletion of solvent molecules around ''sol-

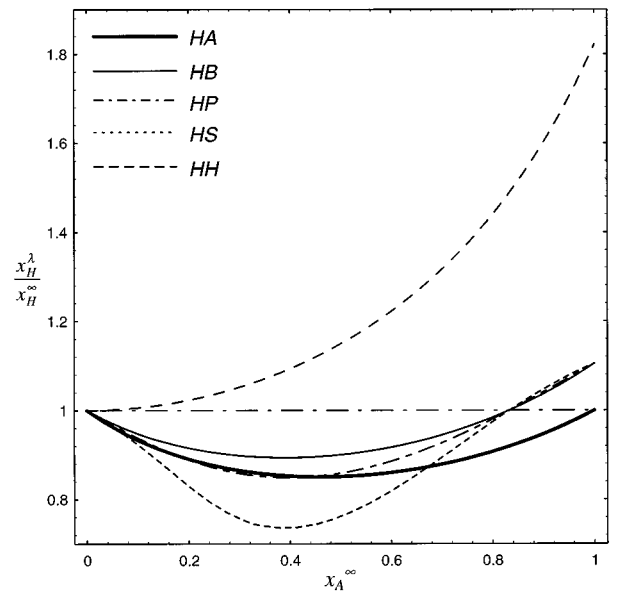

FIG. 7. Presented are analytical solutions for a lattice gas (i.e., *A*-monomers and holes in the bulk) where *H*-holes are adsorbed in the first layer of different reference sites. Ratios of local densities to bulk densities, x_H^λ/x_H^∞, are shown as a function of the bulk density of *A*-monomers, x_A^∞. Case *HA* represents the local densities of *H*-holes around *A*-monomers ($\lambda=A$) and case *HH* represents the local densities of *H*-holes and *H*-holes ($\lambda=H$). The other three cases show local densities of *H*-holes around different ''solutes'' (*B*-monomer, *P*-polymer, *S*-surface). Case *HB* represents the local densities of *H*-holes around a *B*-monomer ($\lambda=B$) in infinite dilution. Case *AP* represents the local densities of *H*-holes around a *P*-polymer ($\lambda=P$) in infinite dilution and case *AS* shows the local densities of *H*-holes at a *S*-surface ($\lambda=S$). For the analytical calculations Eq. (26) is used with the values in Table III. The interaction energies are identical to those in Figs. 4 and 5, i.e., the *A*-monomer self-interactions are slightly stronger than the interactions between *A*-monomers and ''solutes'' (*B*-monomers, *P*-polymer, *S*-surface). The values are $\epsilon_{AB}=\epsilon_{AP}=\epsilon_{AS}=-0.5\ k_BT$ and $\epsilon_{AA}=-0.6\ k_BT$.

utes'' results in a depletion and enhancement of holes around ''solutes.'' This is illustrated in Fig. 7.

Figure 7 shows ratios of local densities of holes to be bulk density of holes, x_H^λ/x_H^∞, as a function of the bulk density of solvent, x_A^∞. The case for hole–hole interactions (HH) is the mirror image of that for solvent–solvent interactions (AA) shown in Figs. 3 and 4. Figure 7 illustrates that the environment around holes is random at low bulk densities, but that there is significant clustering of the holes at high densities. Figure 7 also shows the preferential clustering of holes around solute molecules at high densities. Therefore, even though the solvent–solvent interactions approach random behavior at high densities, the solvent-solute interactions do not.

ACKNOWLEDGMENTS

The authors would like to acknowledge support by the Division of Chemical Sciences of the Office of Basic Energy Sciences, U.S. Department of Energy, under Contract No. DE-FG02-87ER13777, and support by the Chemical and Thermal Systems division of the National Science Foundation under Grant No. CTS-9313714.

APPENDIX A: THREE MATHEMATICALLY EQUIVALENT EXPRESSIONS FOR THE CONFIGURATIONAL ENERGY OF A LATTICE GAS

The configurational energy is given by the sum over all nearest-neighbor interaction energies. For a lattice gas, i.e., a mixture of *A*-monomers and *H*-holes, U can be written as

$$U=\epsilon_{AA}\sum_{i=1}^{N_A} z_i^A/2 = \epsilon_{AA}N_{AA}, \tag{A1}$$

where z_i^A denotes the number of A molecules around the ith A molecule, N_A the total number of A molecules, and N_{AA} the total number A-A bonds. Since the maximum number of A-A bonds is given by $N_Az/2$ (when N_A is a large number, so that boundary effects can be neglected), the probability for having an A-A bond is given by

$$x_A^A=\frac{N_{AA}}{N_Az/2}. \tag{A2}$$

Insertion of Eq. (A2) into Eq. (A1) leads to

$$\widetilde{U}=\widetilde{\epsilon}x_A^A, \tag{A3}$$

where the dimensionless internal energy, $\widetilde{U}=U/U_{\rm kin}$, $U_{\rm kin}=k_BTN_Az/2$, and the dimensionless interaction energy, $\widetilde{\epsilon}=\epsilon_{AA}/k_BT$, were used. Alternative expressions of Eq. (A3) can be obtained by applying the conservation laws

$$\tfrac{z}{2}N_A=N_{AA}+\tfrac{1}{2}N_{AH}, \tag{A4}$$

and

$$\tfrac{z}{2}N_H=N_{HH}+\tfrac{1}{2}N_{AH}. \tag{A5}$$

Replacing N_{AA} in Eq. (A1) by Eq. (A4) leads to

$$U=\tfrac{z}{2}N\epsilon_{AA}(x_A^\infty-\tfrac{1}{2}P_{AH}), \tag{A6}$$

where P_{AH} is the probability for having an A-H bond, given by

$$P_{AH}=x_A^\infty(1-x_A^A)+(1-x_A^\infty)(1-x_H^H). \tag{A7}$$

Combining Eqs. (A6) and (A7) results in

$$\widetilde{U}=\widetilde{\epsilon}\{1-\tfrac{1}{2}[(1-x_A^A)+(1-x_A^\infty)/x_A^\infty(1-x_H^H)]\}. \tag{A8}$$

Note that Eq. (A8) can be obtained directly from Eq. (17). Replacing N_{AA} in Eq. (A1) by Eq. (A4) and N_{AH} by Eq. (A5), leads to

$$\widetilde{U}=\widetilde{\epsilon}[1-(1-x_A^\infty)/x_A^\infty(1-x_H^H)]. \tag{A9}$$

By comparing Eq. (A3) with Eq. (A9), one obtains the equality

$$x_A^\infty(1-x_A^A)=(1-x_A^\infty)(1-x_H^H), \tag{A10}$$

discussed previously. Although Eqs. (A3), (A8), and (A9) are mathematically equivalent to each other, they lead to slightly different results when approximations for the local densities (i.e., x_A^A and x_H^H) are used.

This is demonstrated in Figs. 8 and 9, where approximations for x_A^A and x_H^H were calculated from the Ono–Kondo equation (12). Figure 8(a) shows the resulting approximate

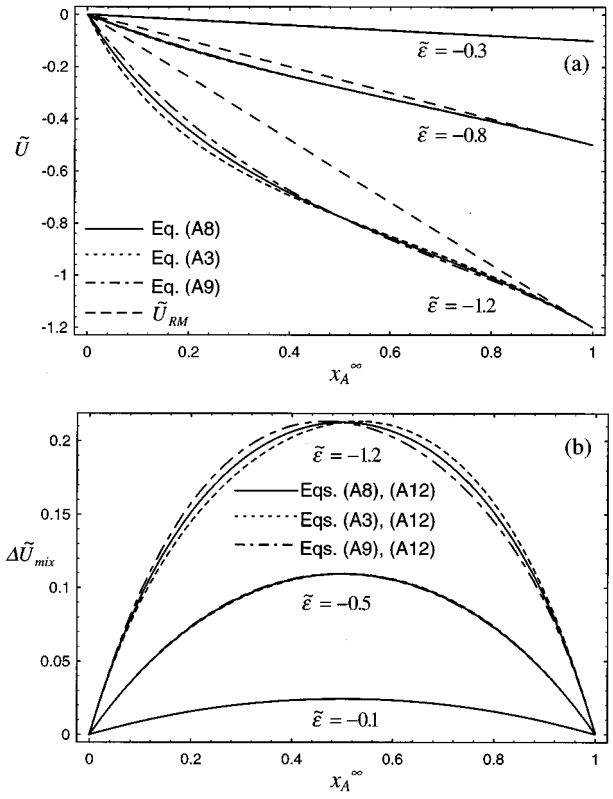

FIG. 8. The internal energy for a lattice gas is presented as a function of the bulk density for three different interaction energies. In (a) approximate solutions of Eqs. (A3), (A8), and (A9), where local densities were obtained from the Ono–Kondo equation (12), are shown together with the internal energy for a random lattice gas, Eq. (A11). In (b), the internal energy of mixing, Eq. (A12), is given for the approximate solutions of Eqs. (A3), (A8), and (A9).

solutions of Eqs. (A3), (A8), and (A9) for three different interaction energies, together with the internal energy for the random mixture,

$$\tilde{U}_{RM} = \tilde{\epsilon} x_A^\infty . \tag{A11}$$

For $\tilde{\epsilon} = -0.3$ and $\tilde{\epsilon} = -0.8$, the results for Eqs. (A3), (A8), and (A9) are practically identical, whereas for $\tilde{\epsilon} = -1.2$, deviations among them can be seen. However, these deviations still are small, compared to those between the internal energy for the random and the nonrandom mixture.

In Fig. 8(b), the internal energy of mixing, $\Delta\tilde{U}_{\rm mix}$, given by

$$\Delta\tilde{U}_{\rm mix} = \frac{U - U_{\rm pure}}{N k_B T z/2}, \tag{A12}$$

with

$$U_{\rm pure} = \tilde{\epsilon} N k_B T z / 2 x_A^\infty , \tag{A13}$$

is shown for the approximate solutions of Eqs. (A3), (A8), and (A9) for the same interaction energies as in Fig. 8(a). As expected, differences between the approximate solutions become more obvious for the internal energy of mixing. It also can be seen that the approximate solution of Eq. (A8) leads to symmetric curves, since it averages Eqs. (A3) and (A9).

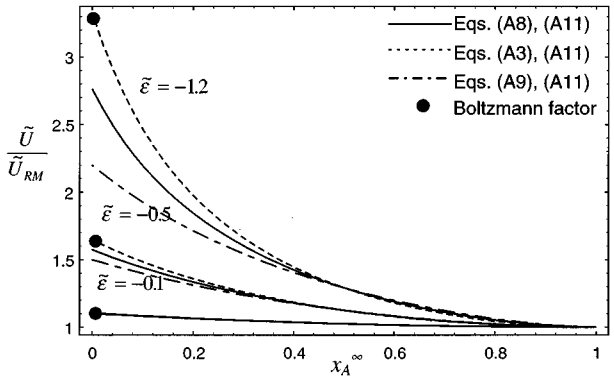

FIG. 9. The ratio of the internal energy for a nonrandom lattice gas to the internal energy of a random lattice gas is presented as a function of the bulk density. Approximations for the nonrandom internal energy were calculated from Eqs. (A3), (A8), and (A9), by applying the Ono–Kondo equation (12).

The approximations from Eqs. (A3) and (A9) are symmetric to each other with respect to the symmetry line at a bulk density of 0.5.

In Fig. 9, the ratio of the internal energy for a nonrandom lattice gas to the internal energy of a random lattice gas is shown as a function of the bulk density. Approximate solutions for the internal energy for the nonrandom system are calculated from Eqs. (A3), (A8), and (A9), by applying the Ono–Kondo equation, Eq. (12). The points denote Boltzmann factors, $\exp(-\tilde{\epsilon})$, for three different interaction energies, which represents the correct low density limit. All solutions show the correct limit for the bulk density going to unity. However, only the approximate solution from Eq. (A3) shows the correct limit for the density going to zero, whereas the approximate solutions from Eqs. (A8) and (A9) deviate from the Boltzmann factor. This trend increases with increasing interaction energy or decreasing temperature. Although the correct high density limit is reached by all three curves, this limit is approached slightly differently.

APPENDIX B: EQUATION FOR LOCAL DENSITIES FOR A LATTICE GAS

Adsorption of monomer around solutes

Adopting the general form of the equation for local densities in fluids, Eq. (26), to a binary system, where we only have A-monomers ($i = A$) and H-holes ($l = H$) in the bulk, leads to the following simplifications:

$$x_i^\lambda = x_A^\lambda , \quad x_l^\lambda = x_H^\lambda = 1 - x_A^\lambda , \tag{B1}$$

$$x_i^\infty = x_A^\infty , \quad x_l^\infty = x_H^\infty = 1 - x_A^\infty , \tag{B2}$$

$$\epsilon_{i\lambda} = \epsilon_{A\lambda} , \quad \epsilon_{l\lambda} = \epsilon_{H\lambda} = 0, \tag{B3}$$

$$\sum_{m=1}^{\nu} x_m^\lambda (\epsilon_{im} - \epsilon_{lm}) = x_A^\lambda (\epsilon_{AA} - \epsilon_{AH}) + x_H^\lambda (\epsilon_{AH} - \epsilon_{HH}), \tag{B4}$$

$$\sum_{m=1}^{\nu} x_m^{\infty}(\epsilon_{im}-\epsilon_{lm}) = x_A^{\infty}(\epsilon_{AA}-\epsilon_{AH}) + x_H^{\infty}(\epsilon_{AH}-\epsilon_{HH}). \tag{B5}$$

Since $\epsilon_{AH}=\epsilon_{HH}=0$, Eqs. (B4) and (B5) simplify to

$$\sum_{m=1}^{\nu} x_m^{\lambda}(\epsilon_{im}-\epsilon_{lm}) = x_A^{\lambda}\epsilon_{AA}, \tag{B6}$$

$$\sum_{m=1}^{\nu} x_m^{\infty}(\epsilon_{im}-\epsilon_{lm}) = x_A^{\infty}\epsilon_{AA}. \tag{B7}$$

For convenience, we introduce $\widetilde{K}_2 \equiv (z-K_2)$. Inserting Eqs. (B1), (B2), (B3), (B6), and (B7) into Eq. (26) gives

$$k_B T \ln\left(\frac{x_A^{\lambda}}{(1-x_A^{\lambda})}\frac{(1-x_A^{\infty})}{x_A^{\infty}}\right) + \epsilon_{A\lambda} + K_1 x_A^{\lambda}\epsilon_{AA} - \widetilde{K}_2 x_A^{\infty}\epsilon_{AA} = 0. \tag{B8}$$

After a rearrangement, Eq. (B8) can be written as

$$x_A^{\lambda} = \frac{x_A^{\infty}}{x_A^{\infty} + (1-x_A^{\infty})\exp\{[\epsilon_{AA}(K_1 x_A^{\lambda} - \widetilde{K}_2 x_A^{\infty}) + \epsilon_{A\lambda}]/k_B T\}}. \tag{B9}$$

Adsorption of holes around solutes

We rearrange Eq. (B8) by replacing x_A^{λ} with $1-x_H^{\lambda}$ and x_A^{∞} with $1-x_H^{\infty}$. The result is

$$x_H^{\lambda} = 1 - \frac{x_A^{\infty}}{x_A^{\infty} + (1-x_A^{\infty})\exp\{[\epsilon_{AA}(K_1(1-x_H^{\lambda}) - \widetilde{K}_2 x_A^{\infty}) + \epsilon_{A\lambda}]/k_B T\}}. \tag{B10}$$

A special case for holes in the first shell of a reference site is the adsorption of holes around holes. In this case, $\epsilon_{A\lambda} = \epsilon_{AH} = 0$, and Eq. (B10) simplifies to

$$x_H^{\lambda} = 1 - \frac{x_A^{\infty}}{x_A^{\infty} + (1-x_A^{\infty})\exp\{\epsilon_{AA}(K_1(1-x_H^{\lambda}) - \widetilde{K}_2 x_A^{\infty})/k_B T\}}. \tag{B11}$$

[1] G. L. Aranovich and M. D. Donohue, J. Chem. Phys. **105**, 7059 (1996).

[2] S. Ono and S. Kondo, *Molecular Theory of Surface Tension in Liquids* (Springer, Göttingen, 1960).

[3] J. S. Rowlinson and B. Widom, *Molecular Theory of Capillarity* (Clarendon Press, Oxford, 1982).

[4] G. L. Aranovich and M. D. Donohue, J. Coll. Int. Sci. **188** (1997).

[5] T. L. Hill, *An Introduction to Statistical Thermodynamics* (Dover, New York, 1986).

[6] G. L. Aranovich and M. D. Donohue, J. Chem. Phys. **104**, 3851 (1996).

[7] M. D. Donohue and P. Vimalchand, Fluid Phase Equilib. **40**, 185–211 (1988).